12th International Symposium on Turbulence and Shear Flow Phenomena (TSFP12)
Osaka, Japan (Online), July 19-22, 2022

PREDICTION AND CONTROL OF TURBULENT FLOWS USING DEEP LEARNING

Jiyeon Kim
School of Mathematics and Computing
(Computational Science and Engineering)
Yonsei University
Seoul 03722, Korea
jykim3994@yonsei.ac.kr

Junhyuk Kim
Department of Mechanical Engineering
Yonsei University
Seoul 03722, Korea
junhyuk6@yonsei.ac.kr

Changhoon Lee
School of Mathematics and Computing (Computational Science and Engineering)
Department of Mechanical Engineering
Yonsei University
Seoul 03722, Korea
clee@yonsei.ac.kr

ABSTRACT

In this study, prediction and control of 2D decaying homogeneous isotropic turbulence (DHIT) using deep learning have been performed as an example of a fundamental study to improve understanding of the dynamic behavior of turbulence. PredictionNet, a neural network used for prediction, showed high accuracy in the prediction of flow up to one integral time scale, T_L, with a correlation coefficient of 0.855. Our model based on generative adversarial network (GAN) also showed much higher accuracy in the enstrophy spectrum than convolutional neural network (CNN) model. Predicability depending on the scale is also analyzed using scale decomposition. Another neural network used for control, ControlNet, was able to generate disturbances that allow the time-evolution of the flow field to be in a direction that fits the objective function. In addition, it was possible to bring some physical understanding of the input vorticity fields through the analysis of the disturbance fields.

INTRODUCTION

Recently, a lot of studies applying data-driven learning to various applications in turbulence such as flow control (Yeh *et al.*, 2021), closure modeling (Maulik *et al.*, 2018), and flow reconstruction (Deng *et al.*, 2019) are actively conducted. However, there are not many examples yet of turbulence prediction and control, especially for the time-varying turbulence, due to complex characteristics such as high-dimensionality, multi-scale, and nonlinearity. Thus, we tried to develop a prediction model using GAN (Goodfellow *et al.*, 2014) that predicts the evolution of turbulence with high accuracy by reflecting not only spatial information but also statistical characteristics of turbulence and to present a control model which enables turbulence control for some specific purposes using this high-accuracy prediction model as a surrogate model. Although it is a prediction and control of a relatively simple 2D turbulence, the results of the current study provide a new approach to prediction and flow control that can be applied to practical applications and more complex turbulence.

MACHINE LEARNING METHODOLOGY

In this section, target, loss function, applied model and network architecture of PredictionNet and ControlNet will be explained.

PredictionNet

We applied two models of CNN and conditional GAN (cGAN, Mirza & Osindero, 2014) for PredictionNet. CNN was used as a baseline model because it is well known for its capability of learning spatial information of variables embedded in data. However, CNN has a problem of producing blurry output sometimes due to the objective function which is simply minimizing the mean squared difference of the ground truth and the prediction (Kim & Lee, 2020; Kim *et al.*, 2021). On the other hand, GAN returns a well-trained generator (G) containing statistical aspects of the data through adversarial training to a discriminator (D). In the basic GAN, the parameters of G and D are updated in directions to minimize $\log(1-D(G(\boldsymbol{z})))$ and $\log(D(\boldsymbol{x}))$, respectively, which stands for the two-player min-max game with value function, $V(G,D)$:

$$\begin{aligned}\min_G \max_D V(G,D) &= \mathbb{E}_{\boldsymbol{x}\sim p(\boldsymbol{x})}\left[\log D(\boldsymbol{x})\right] \\ &+ \mathbb{E}_{\boldsymbol{z}\sim p(\boldsymbol{z})}\left[\log(1-D(G(\boldsymbol{z})))\right]\end{aligned} \tag{1}$$

First, for the cGAN model used in this study, eq.(1) is modified using Earth-Mover (Wasserstein-1) distance (WGAN, Arjovsky *et al.*, 2017) to stabilize the training procedure. Then, some extra information, $\boldsymbol{y}$, the input of the generator in our case, is given as a condition to the input of the discriminator to

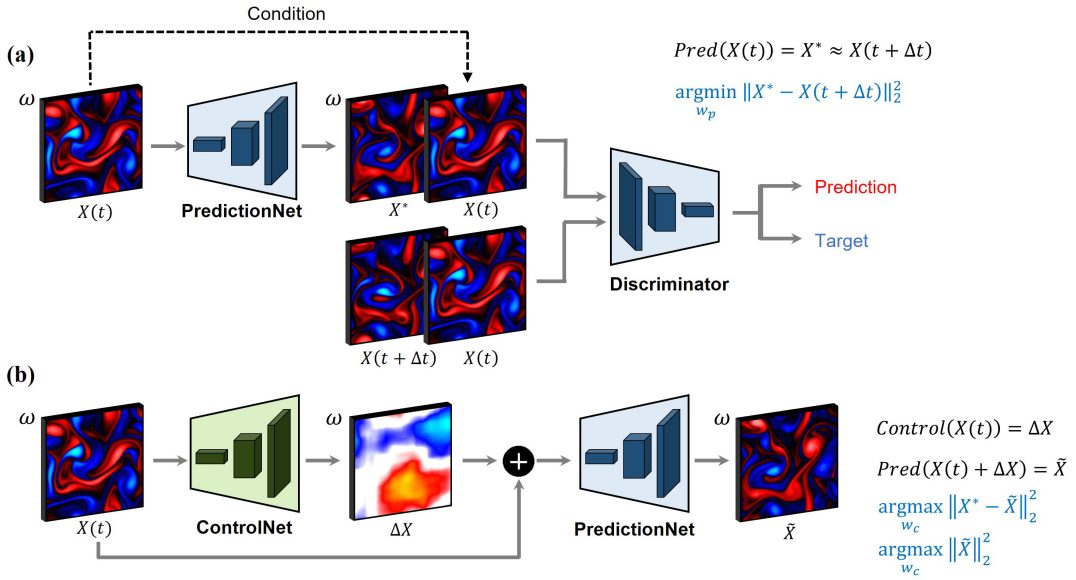

Figure 1. Schematic configurations of (a) PredictionNet and (b) ControlNet.

improve the output quality of the generator like the following:

$$\begin{aligned}\min_G \max_D V(G,D) &= \mathbb{E}_{\boldsymbol{x}\sim p(\boldsymbol{x})}\left[D(\boldsymbol{x}\mid \boldsymbol{y})\right] \\ &- \mathbb{E}_{\boldsymbol{z}\sim p(\boldsymbol{z})}\left[D(G(\boldsymbol{z}\mid \boldsymbol{y}))\right].\end{aligned} \tag{2}$$

PredictionNet is a network that predicts the vorticity field of a later time, Δt, from an input field ($Pred(X(t_i)) = X_i^* \approx X(t_i+\Delta t)$). It is trained using direct numerical simulations (DNS) data to play a functional role in predicting the later time from each time point of our dataset. Therefore, the following objective function is the optimization target regardless of the applied model:

$$\underset{w_p}{\text{argmin}} \|X_i^* - X(t_i+\Delta t)\|_2^2 \tag{3}$$

where X and X^* represent the real (DNS) data and prediction result, respectively, and w_p means weight parameters of PredictionNet. Based on the objective function eq.(3), additional terms such as regularization loss or adversarial loss are added to form loss functions depending on the model applied. For CNN, an L2 regularization loss is used to prevent overfitting and increase stability as follows:

$$\begin{aligned}L_{CNN} &= \frac{1}{N}\sum_{i=1}^{N} L_i + \sigma R(w_p) \\ L_i &= \left\langle (\omega_i^* - \omega_{t_i+\Delta t})^2 \right\rangle \quad R(w_p) = \frac{1}{2}\sum_k w_{p,k}^2\end{aligned} \tag{4}$$

where N and σ are the batch size and the strength of regularization, each of which is set to 32 and 0.0001 by fine-tuning. The loss function of cGAN was set by adding a gradient penalty (GP) loss term (WGAN-GP, Gulrajani *et al.*, 2017) based on eq.(2) as follows:

$$\begin{aligned}L_{cGAN} &= \gamma \frac{1}{N}\sum_{i=1}^{N} L_i - L_{adv} \\ L_i &= \left\langle (\omega_i^* - \omega_{t_i+\Delta t})^2 \right\rangle \quad L_{adv} = L_{false}\end{aligned} \tag{5}$$

$$\begin{aligned}L_D &= -L_{true} + L_{false} + \alpha L_{gp} + \beta L_{drift} \\ L_{true} &= \frac{1}{N}\sum_{i=1}^{N} D(\omega_{t_i+\Delta t}, \omega_{t_i}) \quad L_{false} = \frac{1}{N}\sum_{i=1}^{N} D(\omega_i^*, \omega_{t_i})\end{aligned} \tag{6}$$

where α, β, and γ determine the portion of each loss term in the total loss, and fixed to 100, 10, and 0.001. The schematic configuration of PredictionNet can be found from figure 1(a). One thing to note that is if there's no discriminator then it is the configuration of the baseline CNN model.

ControlNet

For ControlNet, the same generative CNN as baseline CNN or cGAN generator of PredictionNet was used. ControlNet is trained to generate disturbance fields that fit the objective function combined with PredictionNet ($Control(X(t_i)) = \Delta X_i$, $Pred(X(t_i)+\Delta X_i) = \tilde{X}_i$). Examples of the objective function used in this study include maximizing the change of vorticity at a later time (propagation of control effect) and minimizing the enstrophy at a later time as follows:

$$\underset{w_c}{\text{argmax}} \|X_i^* - \tilde{X}_i\|_2^2 \tag{7}$$

$$\underset{w_c}{\text{argmin}} \|\tilde{X}_i\|_2^2 \tag{8}$$

where $\tilde{X}$ and w_c are disturbed prediction at time $t+\Delta t$ and weight parameters of ControlNet, respectively. A spatial gradient loss term is additionally used to remove non-physical

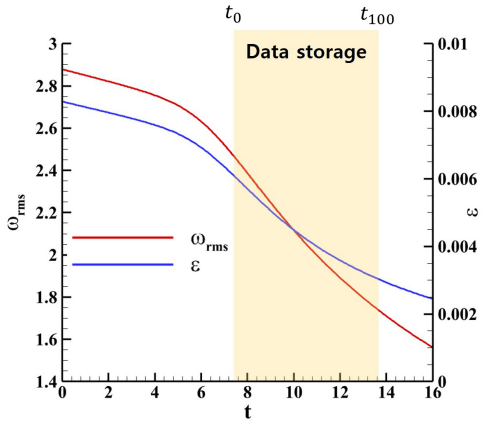

Figure 2. The decaying level of vorticity RMS and dissipation rate within the dataset time interval, $100\delta t$.

noise for the ControlNet loss function as follows:

$$L_{control} = \frac{1}{N}\sum_{i=1}^{N} L_i + \theta L_{grad}$$

$$L_{grad} = \frac{1}{N}\sum_{i=1}^{N}\left[\left\langle\left(\frac{\omega_{t_t}^{p+1,q}-\omega_{t_i}^{p,q}}{dx}\right)^2\right\rangle + \left\langle\left(\frac{\omega_{t_i}^{p,q+1}-\omega_{t_i}^{p,q}}{dy}\right)^2\right\rangle\right] \quad (9)$$

The schematic configuration of ControlNet can be found from figure 1(b).

DATA COLLECTION

Because the flow is 2-dimensional, DNS were performed on the incompressible Navier-Stokes equations in the form of the vorticity transport equation and the stream function formulation to basically satisfy the continuity equation, as follows:

$$\frac{\partial\omega}{\partial t} = -u_j\frac{\partial\omega}{\partial x_j} + \nu\frac{\partial^2\omega}{\partial x_j\partial x_j} \quad \& \quad \frac{\partial^2\psi}{\partial x_j\partial x_j} = -\omega \quad (10)$$

where ω, ψ, and ν are vorticity, stream function, and kinematic viscosity, respectively. They are solved by the pseudo-spectral method with 3/2 zero-padding for de-aliasing. The simulation time step, dt, is 0.0025, and the Crank-Nicolson method for the viscous term and the 2nd order Adams-Bashforth method for the convective term are used for the time integration. Computational domain size is $2\pi\times2\pi$, the number of spatial grids is 128×128, and the bi-periodic boundary condition is applied spatially. 500, 100, and 50 independent simulations with random phase and fixed amplitude initialization are performed for training, validation and test, respectively. The time interval of the dataset was determined after statistically sufficiently developed (after satisfying the power-law spectrum), and the data time step, δt, equals 20 simulation time steps ($\delta t = 20dt$). Although we are reflecting the decaying nature of the flow in our models, it is undesirable if those flow fields almost converged to the steady solution were contained in the dataset. So, only $100\delta t$ interval showing a relatively high rate of change in statistics is chosen. Among the representative statistics, the root mean square (RMS) of vorticity decreased by about 25% and dissipation rate (ϵ) decreased by about 44% in this interval (see figure 2).

Table 1. Quntified predictive accuracy of CNN and cGAN by test MSE & C.C. depending on the prediction time distance.

	Test MSE		C.C.	
Δt	CNN	cGAN	CNN	cGAN
$0.25T_L$	0.0144	0.0086	0.9898	0.9940
$0.5T_L$	0.0404	0.0390	0.9699	0.9708
T_L	0.1298	0.1724	0.8870	0.8547
$2T_L$	0.3863	0.5056	0.5227	0.4530

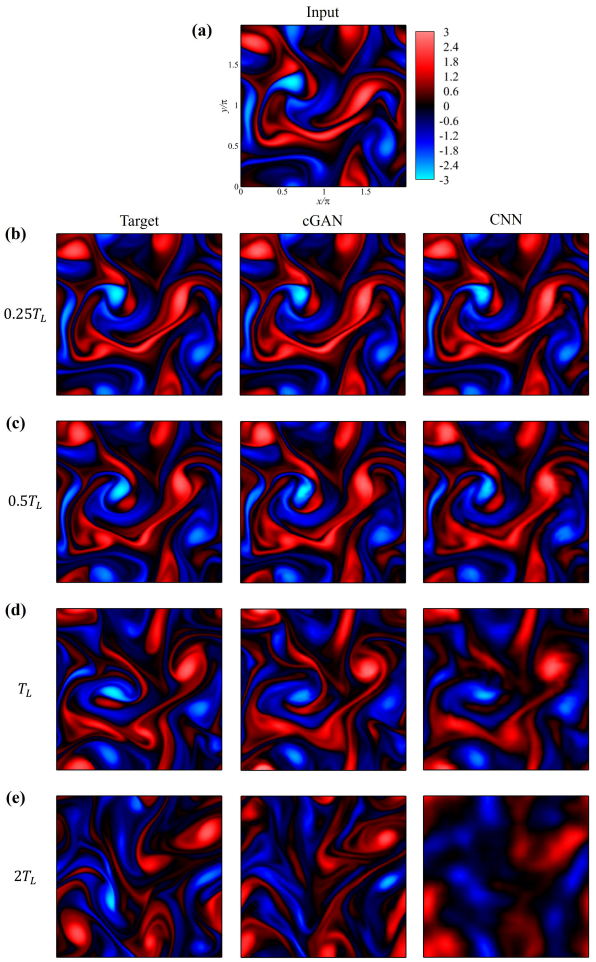

Figure 3. Examples of PredictionNet result using one of test simulations. (a) Input field. And results of prediction time distances of (b) $\Delta t = 0.25T_L$, (c) $\Delta t = 0.5T_L$, (d) $\Delta t = T_L$, and (e) $\Delta t = 2T_L$.

RESULTS

PredictionNet

The prediction results of PredictionNet were compared according to the prediction time distance, Δt. It is set to 0.25, 0.5, 1, and 2 times the integral time scale, T_L. It corresponds to around $40\delta t$ or $800dt$ where the autocorrelation drops to around 0.25. As a result, it was confirmed that both CNN and cGAN show high accuracy in both qualitative and quantitative measures up to one T_L (see Table 1, figure 3). However, as shown in enstrophy spectra of figure 4, it was found that CNN failed to predict the high-wavenumber region even from a very close Δt. On the other hand, in the case of cGAN, high-order

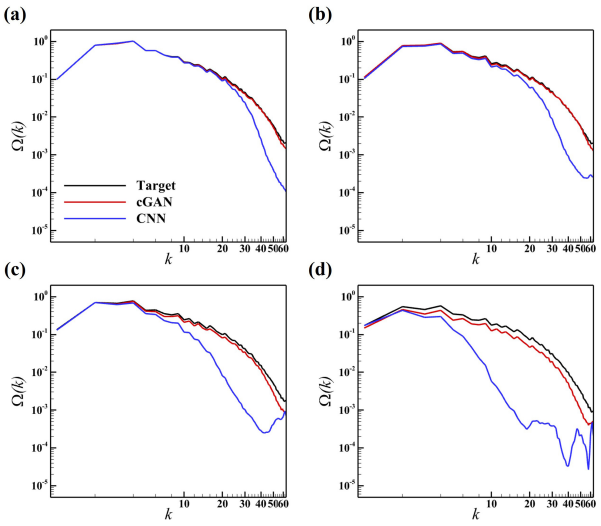

Figure 4. Comparison of enstrophy spectra for the input time point of t_0. (a) $\Delta t = 0.25T_L$, (b) $\Delta t = 0.5T_L$, (c) $\Delta t = T_L$, and (d) $\Delta t = 2T_L$.

statistics are predicted well only with a small amount of error even at T_L.

It is conjectured that cGAN reflects the statistical characteristics of the target flow field well while the generator is trained adversarially to the discriminator and contains the spatial correlation between the input and the target by conditioning the discriminator to take the input field of the generator together with its own inputs (i.e., the prediction target and the generated flow field). In other words, cGAN seems to contain small-scale characteristics better by learning the non-linear features of the flow field based on complex dynamics compared to CNN that simply minimizes MSE based on point-wise values. This can be verified using scale decomposition as shown in figure 5. While CNN fails to generate small-scale details and underpredicts even intermediate-scale features, cGAN shows very high accuracy for both large-scale and intermediate-scale. Small-scale details are also generated well, although the structures are slightly shifted and distorted.

ControlNet

The first target of ControlNet is to maximize the propagation of the control effect at a later time, as in eq.(7). Here, we set the target time distance as $0.5T_L$, and the only constraint applied to ControlNet is the RMS of the disturbance field ($\Delta X_{rms} = 0.05X_{rms}$). Looking at the disturbance field and enstrophy spectra in figures 6(c) and 6(e), a disturbance with large-scale structures in which most of the energy is concentrated in the low-wavenumber region is generated. In addition, this energy-concentrated disturbance structures are mostly acting on the vortex structures of the input field. Thus, we can think of it as the control effect of ControlNet output is propagated and amplified well to the later time by transposing the dynamic path of the flow evolution. As a result, it is shown that the vortex structures of original prediction and disturbance added prediction have slightly different positions and directions (see figures 6(b) and 6(d)). To see whether our disturbance is the optimum case for maximizing the change of vorticity field under the given condition, we performed two separate validation cases. The first one is shown in figure 7(a), showing the results of quantifying the degree of change at the

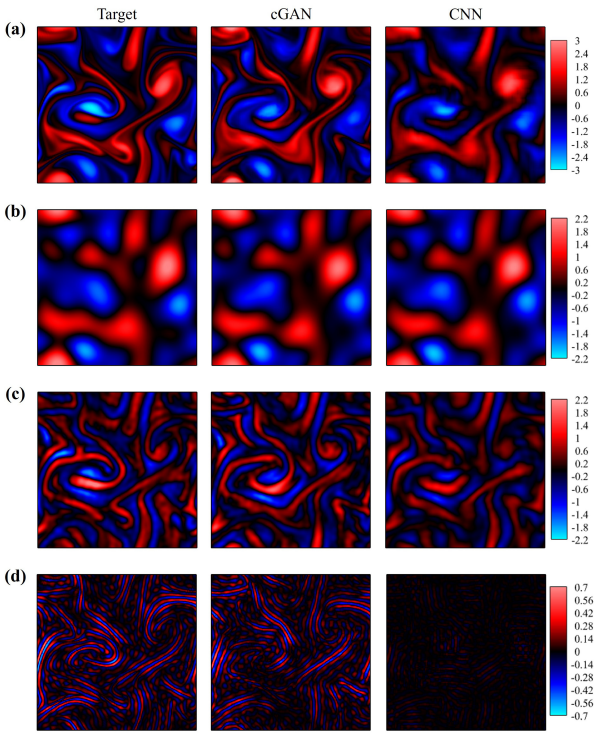

Figure 5. Results of scale decomposition for $\Delta t = T_L$. (a) Original fields, (b) large-scales ($k \leq 4$), (c) intermediate-scales ($5 \leq k \leq 20$), and (d) small-scales ($k \geq 21$).

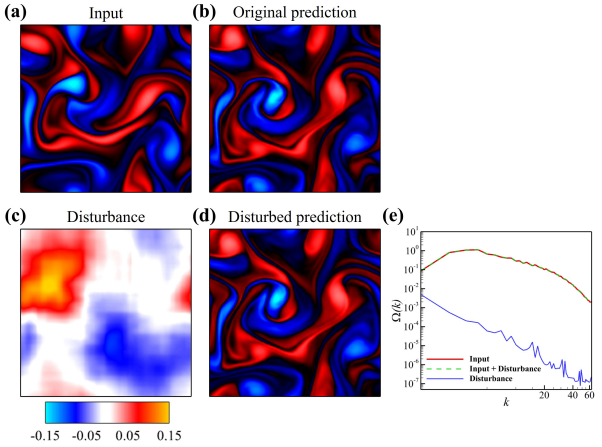

Figure 6. Examples of ControlNet with the target $\mathrm{argmax}_{w_c} \|X_i^* - \tilde{X}_i\|_2^2$. (a) Input field, (b) original prediction, (c) disturbance field, (d) disturbance added prediction, and (e) enstrophy spectra.

later time from the original prediction by MSE. The ControlNet output, red dotted line, is the largest control effect compared to the subsequent 1000 nodes, MSE using other disturbance fields modified by random phase shift or spatial shift. The second one is shown in figure 7(b). It presents normalized RMS difference of simulations by adding various disturbance fields to the input, including disturbances suggested by previous researches, from the original simulation. Obviously, the best case was our ControlNet output (red line).

The second target is to minimize the enstrophy at a later time, as in eq.(8). Looking at the disturbance field and enstrophy spectra in figures 8(c) and 8(e), we can see that disturbance with an almost similar structure to the main vortex structures

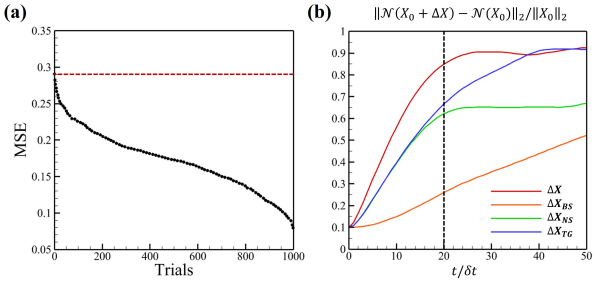

Figure 7. (a) Quantifed results about the degree of the propagation of the control effect by MSE, and (b) normalized RMS difference of various simulations from the original simulation.

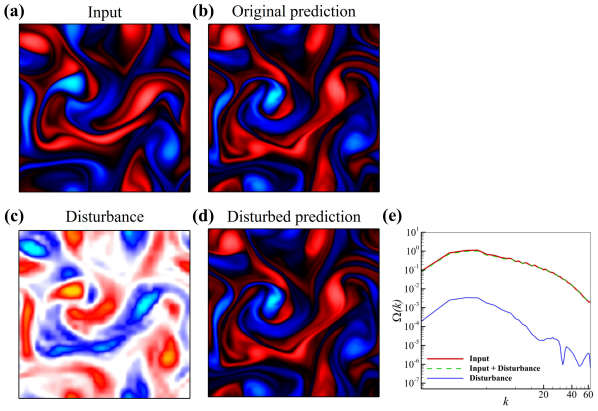

Figure 8. Examples of ControlNet with the target $\mathrm{argmin}_{w_c} \|\tilde{X}_i\|_2^2$. (a) Input field, (b) original prediction, (c) disturbance field, (d) disturbance added prediction, and (e) enstrophy spectra.

of the input field but in opposite sign is generated. The spectrum also showed a very similar result to the input. Checking the disturbed prediction fields, there was only minor change in the behavior and evolution of the flow field, and only the rate of decay and min/max values are affected to minimize enstrophy at the later time.

CONCLUSION

In this study, prediction and control of 2D decaying turbulence were performed as a fundamental example of prediction and control of turbulence. In the prediction part, models that can predict with high accuracy up to a time where the turbulence is temporally decorrelated were developed. Among them, the cGAN model was able to predict even small-scale features well by reflecting the complex nonlinear dynamics and interactions of turbulence, and scale decomposition that can more precisely analyze the accuracy of turbulence prediction is presented. In the control part, we developed a model that can produce a control effect suitable for the desired target. Although this study is a fundamental example of a relatively simple flow field, it has the potential to be applied to practical applications or more complex turbulence.

ACKNOWLEDGMENTS

This work was supported by National Research Foundation of Korea (NRF) grants funded by the Korean government (MSIP) (2017R1E1A1A03070282, 2022R1A2C2005538).

REFERENCES

Arjovsky, M., Chintala, S. & Bottou, L. 2017 Wasserstein generative adversarial networks. In *34th ICML* (ed. Doina Precup & Yee Whye Teh), *Proceedings of Machine Learning Research*, vol. 70, pp. 214–223. PMLR.

Deng, Z., He, C., Liu, Y. & Kim, K. C. 2019 Super-resolution reconstruction of turbulent velocity fields using a generative adversarial network-based artificial intelligence framework. *Phys. Fluids* **31** (12), 125111.

Goodfellow, I., Pouget-Abadie, J., Mirza, M., Xu, B., Warde-Farley, D., Ozair, S., Courville, A. & Bengio, Y. 2014 Generative adversarial nets. In *Adv. Neural Inf. Process. Syst.* (ed. Z. Ghahramani, M. Welling, C. Cortes, N. Lawrence & K. Q. Weinberger), , vol. 27. Curran Associates, Inc.

Gulrajani, I., Ahmed, F., Arjovsky, M., Dumoulin, V. & Courville, A. 2017 Improved training of wasserstein gans. *Preprint* .

Kim, H., Kim, J., Won, S. & Lee, C. 2021 Unsupervised deep learning for super-resolution reconstruction of turbulence. *J. Fluid Mech.* **910**, A29.

Kim, J. & Lee, C. 2020 Deep unsupervised learning of turbulence for inflow generation at various reynolds numbers. *J. Comput. Phys.* **406**, 109216.

Maulik, R., San, O., Rasheed, A. & Vedula, P. 2018 Subgrid modelling for two-dimensional turbulence using neural networks. *J. Fluid Mech.* **858**, 122–144.

Mirza, M. & Osindero, S. 2014 Conditional generative adversarial nets. *arXiv preprint* .

Yeh, C.A., Meena, M. G. & Taira, K. 2021 Network broadcast analysis and control of turbulent flows. *J. Fluid Mech.* **910**, A15.